Acupuncture and Herbal Medicine

A novel cabazitaxel liposomes modified with ginsenoside Rk1 for cancer targeted therapy

Dandan Huang[1], Zhongjie Tang[1], Xiao Pu[1], Tianqi Wang[2], Feiyan Gao[1,*], Chong Li[1,*]

[1]Medical Research Institute, College of Pharmaceutical Sciences, Southwest University, Chongqing, China; [2]Department of Pharmacy, National University of Singapore, Singapore 117545, Singapore

Abstract

Objective: In this study, we aim to enhance the anti-prostate cancer efficacy of cabazitaxel (CTX) and reduce its immunosuppression and systemic toxicity by developing CTX-loaded liposomes modified with ginsenoside Rk1 (Rk1/CTX-Lip).

Methods: Physical and chemical properties of Rk1/CTX-Lip were investigated. We evaluated the biological functions of Rk1/CTX-Lip, both *in vitro* and *in vivo*. A subcutaneous prostate cancer (RM-1)-bearing mouse model was established to study the efficacy of Rk1/CTX-Lip inhibition in tumors. Simultaneously, a *Candida albicans* infection model was established in tumor-bearing mice to study the infection-relieving efficacy of Rk1/CTX-Lip. Finally, biocompatibility and *in vivo* safety of Rk1/CTX-Lip were evaluated.

Results: We successfully prepared Rk1/CTX-Lip, achieving high CTX encapsulation efficiency (97.24 ± 0.75)% and physical stability. Rk1/CTX-Lip demonstrated evasion of macrophage phagocytosis, effective tumor tissue targeting, and a significant reduction (>50%) in average tumor volume compared with Chol/CTX-Lip. Moreover, it relieved the concurrent infection burden and effectively regulated immune organs and cells, demonstrating superior biocompatibility.

Conclusion: Rk1/CTX-Lip presents a promising new therapy for prostate cancer and holds potential for relieving concurrent fungal infections in cancer patients with low immunity.

Keywords: Cabazitaxel, Fungal infection, Ginsenoside Rk1, Liposome-drug delivery system, Prostate cancer

Graphical abstract: http://links.lww.com/AHM/A92.

Introduction

Cabazitaxel (CTX) is a promising second-generation taxane for treating metastatic castration-resistant prostate cancer. Jevtana® (Sanofi, Gentilly, France) is a micellar CTX solution that was approved by the US Food and Drug Administration (FDA) to treat prostate cancer in 2010[1,2]. Owing to its poor affinity for P-glycoprotein (P-gp), CTX has demonstrated antitumor activity not only against docetaxel-sensitive tumor models but also against docetaxel-insensitive tumor models[3–5]. However, similar to docetaxel, CTX has poor solubility in water with low bioavailability *in vivo* and can result in many severe side effects in patients with cancer, such as neutropenia[6], diarrhea[7], and immunosuppression[8]. The risk of immunosuppression significantly heightens susceptibility to lethal fungal infections, a significant cause of mortality in patients with cancer[9–12]. This underscores the need for developing safer and more effective CTX tumor-targeted delivery systems.

Liposomes are mature and efficient drug delivery systems that demonstrates efficient cellular internalization, thereby reducing drug toxicity *in vivo*[13,14]. Further, ginsenosides are known to have various pharmacological activities, such as antitumor[15,16], anti-inflammatory[15,17], and immune regulation effects[18,19]. Additionally, studies have demonstrated that ginsenosides, with a steroid structure similar to that of cholesterol and attached sugar moieties, can replace cholesterol and form liposomes with phospholipids[20] [Supplementary Figure S1, http://links.lww.com/AHM/A91].

Therefore, to address the limitations of CTX, we established CTX-loaded liposomes modified with ginsenoside Rk1 (Rk1/CTX-Lip). Rk1 has a core structure similar to that of cholesterol. The hydrophilic sugar and hydroxyl groups of Rk1 form hydrogen bonds with the acceptor on the polar head of the phospholipid in liposomes, effectively improving their stability and encapsulation efficiency[21]. Moreover, the exposed Rk1 glycosides on the liposomes can reduce the adhesion of plasma proteins, prolonging the circulation time of Rk1/CTX-Lip. Additionally, these glycosided bind to the glucose transporter 1 (GLUT1) protein, which is highly expressed in tumor cells and promotes Rk1/CTX-Lip accumulation in tumor tissues[22]. Furthermore, Rk1 can improve cellular and humoral immunity[18,19], and synergistically enhance

* Corresponding author. Feiyan Gao, E-mail: feiyanyatou@126.com; Chong Li, E-mail: chongli@swu.edu.cn.

Received 7 November 2023 / Accepted 25 January 2024

How to cite this article: Huang DD, Tang ZJ, Pu X, Wang TQ, Gao FT, Li C. A novel cabazitaxel liposomes modified with ginsenoside Rk1 for cancer targeted therapy. Acupunct Herb Med 2024;4(1):113–121. DOI: 10.1097/HM9.0000000000000096

the anti-prostate cancer efficacy of CTX while reducing immunosuppression and hematotoxicity during treatment[23].

Materials and methods

Materials

Ginsenoside Rk1 (BP1474) was purchased from Chengdu Puruifa Technology Co. Ltd. (Chengdu, China; purity >98%). Cabazitaxel (C3390, 98% purity) was purchased from TCI Chemicals (Shanghai, China). 3-(4,5-Dimethylthiazol-2-y1)2,5-diphenyltetrazolium bromide (Microtetrazolium [MTT], JT343) was purchased from Aladdin (Shanghai, China). Phosphatidylcholine (M3163) was purchased from A.V.T. Pharmaceutical, Ltd. (Shanghai, China). Trypsin solution (0.25%, GP3108) was purchased from Jiangsu Keygen Biotech Co., Ltd. (Jiangsu, China). 4′,6-Diamidino-2-phenylindole (DAPI, GD3408) was purchased from Beijing Dingguo Changsheng Biotechnology Co. Ltd. (Beijing, China). Coumarin-6 (C6) (A2723) and IR-783 (I1031) were purchased from Aladdin (Shanghai, China). The FITC-conjugated anti-CD3 (WP20007), APC-conjugated anti-CD4 (PV6090), and PE-conjugated anti-CD8 (PV5595) antibodies were purchased from Thermo Fisher Scientific (Waltham, MA, UK).

Animals

Female BALB/c mice (5 weeks, 18–22 g) and Sprague Dawley rats 180–220 g were purchased from Hunan Schlechenda Experimental Animal Co., Ltd. (Hunan, China). The animals were maintained in a pathogen-free laboratory animal environment and housed in a controlled environment with a 12-hour light/dark cycle at 22°C to 24°C and 30% to 50% relative humidity.

Preparation and characterization of Rk1/CTX-Lip

Thin film hydration was used to prepare the formulations. The compositions of the prepared formulations were as follows: (1) lecithin/Rk1/CTX (mass ratio, 15:3:1), denoted as Rk1-CTX/Lip; (2) lecithin/Rk1 (mass ratio, 15:3), denoted as Rk1-Lip; and (3) lecithin/cholesterol/CTX (mass ratio, 15:1:1), denoted as Chol/CTX-Lip. All components of the liposomes were dissolved in anhydrous alcohol. Subsequently, alcohol was removed *via* vacuum rotary evaporation. Upon the formation of a thin film layer, it underwent hydrated with ultrapure water and subsequent sonication and membrane extrusion (pore size = 100 nm) to obtain liposomes with a controlled particle size. Dynamic light scattering measurements, performed using a Zetasizer Nano Series (Nano ZS 90, Malvern, UK), characterized particle size and zeta potential. The liposome sample was suspended in phosphate buffer saline (PBS) at a concentration of 1 mg/mL and stored at 4°C for 72 h. Changes in particle size were measured at different time intervals (6, 12, 24, 48, 72 h). All measurements were performed in triplicate at room temperature. Additionally, the surface morphology of the liposomes was analyzed using transmission electron microscopy (TEM) (Ht7800, HITACHI, Tokyo, Japan) after negative staining with 1% phosphotungstic acid. Encapsulation efficiency of CTX was determined by centrifuging the liposomes at 11,000×g for 10 min at 4°C to separate the free CTX. After centrifugation, the liposomes were dissolved in methanol, and the amount of loaded CTX was quantified using high-performance liquid chromatography (HPLC) (Shimadzu, Kyoto, Japan). A mobile phase mixture of water and acetonitrile at a ratio of 40:60 (v/v) was used, and the detection wavelength was set to 230 nm. Encapsulation efficiency was calculated based on the content ratio of encapsulated CTX to the total input amount during fabrication.

In vitro cellular uptake assay

RAW264.7 or RM-1 cells were cultured overnight. Next, C6-labeled liposomes (10 μg/mL) were added to the wells and incubated for 2 h. The cells were then washed thrice with PBS and fixed with 4% paraformaldehyde. Subsequently, the cells were rinsed three times with PBS, and the nuclei were stained using DAPI. Images were captured using a high-content analysis system (Operetta CLS; PerkinElmer, Waltham, MA, USA). Furthermore, C6-labeled liposomes were again added to the wells and incubated for an additional 2 h. After incubation, the cells were washed three times with PBS, digested with trypsin, washed, and resuspended in PBS. Finally, the fluorescence of the cells was measured using FACS (BD, USA). A total of 10,000 cells were analyzed to determine the average cell fluorescence for each replicate.

In vivo and ex vivo liposome distribution by live imaging

Real-time *in vivo* and *ex vivo* fluorescence imaging were performed using Rk1-Lip/IR-783 and Chol-Lip/IR-783. BALB/c mice were subcutaneously inoculated with an ample amount (5×10^7) of RM-1 cells. The respective preparations were administered through the tail vein once the tumor volume reached approximately 100 mm^3. Fluorescence images were captured at predefined intervals. For *ex vivo* imaging, the mice were sacrificed at predetermined time points post-administration. Following that, the major organs (heart, liver, spleen, lungs, kidneys, and brain) and tumors were harvested, cleaned, and visualized using the VISQUE *in vivo* Smart-LF System (Vieworks, Anyang, Korea).

In vivo liposome distribution analysis

Random allocation of RM-1 tumor-bearing mice into three groups was performed, and injection of 100 μL of saline, Rk1-Lip/C6, and Chol-Lip/C6 was administered *via* the tail vein. After 4 h, the mice were sacrificed, and tumor tissues were dissected and embedded in optimal cutting temperature compound. Utilizing a Leica CM1850 cryostat (Leica, Weztlar, Germany), frozen tissue was sliced at a thickness of 10 μm. Sections were then placed on adhesive slides and left at room temperature for 30 min. Subsequently, fixation was performed for 15 min with 4% paraformaldehyde, followed by three immersions in PBS and staining with DAPI for 5 min. Washing with PBS was again performed three

times and imaging was performed using a high-content analysis system. The rats were intravenously injected with the formulations at an equivalent dose of 10 mg/kg CTX to explore the pharmacokinetics of CTX. Blood samples (approximately 0.2 mL) were collected at various time points (15, 30, and 45 min, and 1, 2, 4, 8, 12, and 24 h post-injection) in heparinized centrifuge tubes. Subsequently, centrifugation at 1,500×g for 10 min was performed to separate the plasma, which was then subjected to HPLC analysis. To assess biodistribution, RM-1 tumor-bearing mice were injected through the tail vein with CTX-Sol, Chol/CTX-Lip, or Rk1/CTX-Lip at a dose of 10 mg/kg CTX. The mice were sacrificed at predefined time points (2, 4, 8, and 12 h). Major organs, muscles, and tumors were excised, followed by thorough rinsing with ice-cold saline, drying, and weighing. The tissues were homogenized in a saline solution. Aliquots of 50 µL of plasma or 200 µL of tissue homogenate were mixed with 0.4 mL of methanol containing 10 µL of paclitaxel (used as an internal standard). The mixture was vortexed for 2 min and centrifuged at 6,000×g for 10 min. The supernatant (in methanol) was transferred to a clean tube and dried under a gentle stream of nitrogen. The resulting plasma and tissue residues were re-dissolved in acetonitrile and centrifuged at 11,000×g for 10 min. The supernatant obtained was injected into an HPLC system for analysis.

MTT analysis

The RM-1 cells were cultured overnight in 96-well plates at a seeding density of 2×10^4 cells/well. Subsequently, the cells were treated with various compounds, including CTX, CTX + Rk1, Rk1/CTX-Lip, and Chol/CTX-Lip, for 48 h. After the treatment period, the medium was replaced with fresh complete medium supplemented with an MTT concentration of 0.5 mg/mL. Following a 4 h incubation, the medium was extracted, and the purple formazan crystals formed by the cells were solubilized in 150 µL dimethylsulfoxide (DMSO). Cell viability was determined by measuring the absorbance at 490 nm using a microplate reader (680; Bio-Rad, Hercules, CA, USA).

In vivo antitumor efficacy assay

Mice with RM-1 tumors were randomly divided into four groups ($n = 6$ per group). On days 1, 5, 9, and 13, different preparations, including saline, CTX-Sol, Chol/CTX-Lips, and Rk1/CTX-Lip, were administered *via* the tail vein. To assess the antitumor efficacy of Rk1/CTX-Lip, a dosage of 15 mg/kg CTX was administered simultaneously. Tumor volume was calculated using the formula length × $(\text{width})^2 \times 1/2$, and the body weight of each group was measured every other day. Additionally, the spleen and thymus were removed and weighed to determine the spleen and thymus indices. To examine the proportions of $CD3^+$, $CD4^+$, and $CD8^+$ cells within the tumors, flow cytometric analysis was performed on six tumor samples from each group, considering the tumor heterogeneity.

In vivo fungal burden analysis

Following the *in vivo* administration of Rk1/CTX-Lip to evaluate its antitumor efficacy, a dose of *Candida albicans* (5×10^6) was introduced *via* the tail vein. The mice were sacrificed on days 3 and 7 post-infection, and kidney tissues from each group were meticulously collected, quantified in terms of weight, and homogenized using sterile saline. The resultant homogenate was gradually diluted with sterile saline, and 30 mL of the diluted suspension was plated onto yeast extract peptone dextrose (YDP) medium supplemented with 1% penicillin-streptomycin (in a 1:1 volume ratio). The inoculated plates were then incubated at 30°C for 48 h to facilitate the determination of colony-forming units (CFU) per gram of kidney tissue.

In vivo safety study

Blood samples were collected from mice in each treatment group after removing their eyeballs. These samples were then centrifuged at 4,000 rpm for 10 min, resulting in the separation of the upper serum. Serum levels of various biochemical markers, such as creatinine (CRE), uridylyltransferase (Urea), alanine aminotransferase (ALT) and aspartate aminotransferase (AST), were determined using a biochemical index test kit and an automatic biochemical analyzer (AU400; Olympus Optical Co., Ltd., Tokyo, Japan). Following the sacrifice of the mice in each group, organs, including the brain, heart, liver, spleen, lung, and kidney, were collected for further analysis. Hematoxylin and eosin (H&E) staining was performed on the harvested organs to visualize cellular structures. Additionally, a bone marrow smear was used to assess nucleated cells in the bone marrow. Specifically, bone marrow from the tibia was flushed out and transferred to an objective slide. The cells were counted in a blinded manner by spreading the bone marrow on a coverslip and staining with Giemsa.

Statistical analysis

All data are expressed as the mean ± standard deviation (SD). Statistical analyses were performed using GraphPad Prism 8 (GraphPad, Bethesda, MD, USA). A two-tailed unpaired *t* test was used for comparisons between two groups, and a one-way analysis of variance was used for comparisons between multiple groups. The threshold for statistically significant differences was set at $P < 0.05$.

Results

Preparation and characterization of Rk1/CTX-Lip

Rk1/CTX-Lip was prepared *via* thin film hydration, followed by ultrasonic dispersion. The average hydrodynamic diameter and zeta potential of Rk1/CTX-Lip were measured at (95.15 ± 2.11) nm and (–24.78 ± 1.99) mV, respectively (Figure 1A and Table 1). The lower negative zeta potential of Rk1/CTX-Lip is considered favorable for increasing liposome stability by reducing particle aggregation[24]. The shape of the liposomes was observed by TEM, and the results showed that the liposomes were round with a homogenous size distribution (Figure 1B).

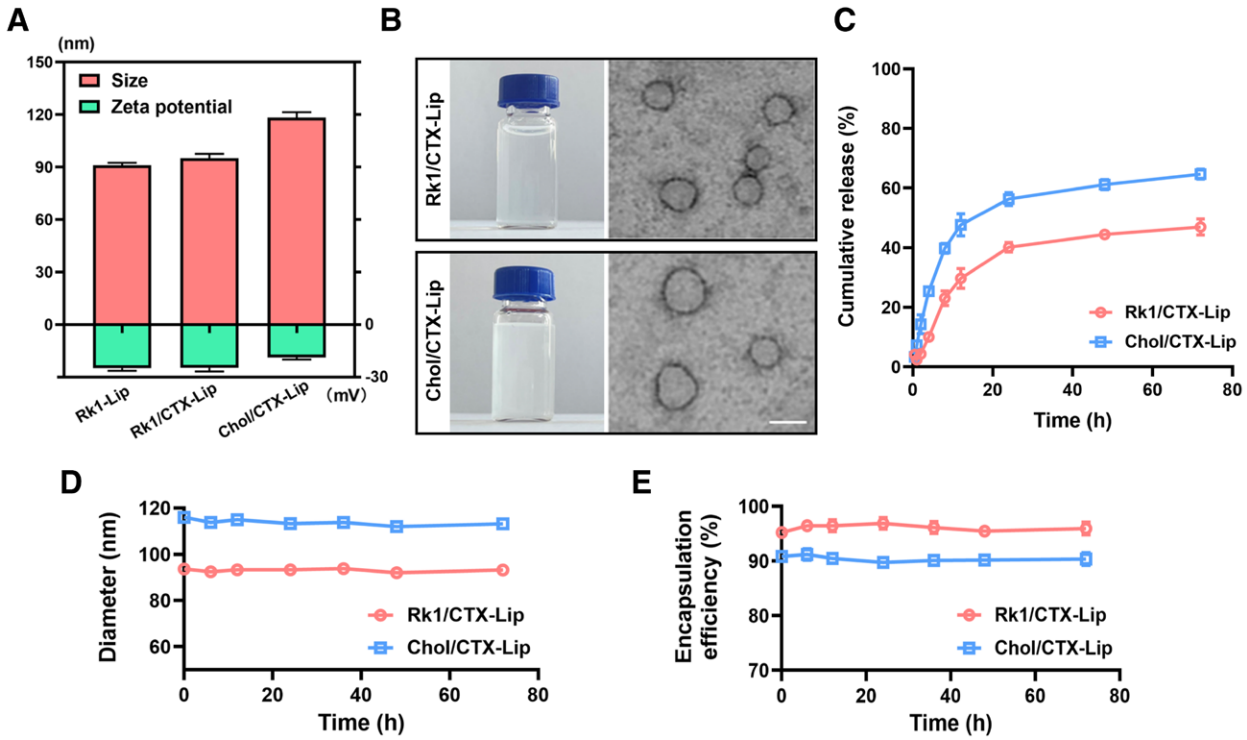

Figure 1. Preparation and characterization of Rk1/CTX-Lip. (A) Hydrodynamic size and zeta potential of Rk1-Lip, Rk1/CTX-Lip, and Chol/CTX-Lip. (B) Appearance and transmission electron micrographs of Rk1/CTX-Lip and Chol/CTX-Lip. Scale bars = 100 nm. (C) *In vitro* CTX release assay of Rk1/CTX-Lip and Chol/CTX-Lip. (D–E) *In vitro* stability (D, Particle size and E, Encapsulation rates) of Rk1/CTX-Lip and Chol/CTX-Lip in saline at 4°C for 72 h. Data represented as mean ± SD (n = 3). Rk1/CTX-Lip: CTX-loaded liposomes modified with ginsenoside Rk1; SD: Standard deviation.

Table 1

Hydrodynamic size and zeta potential of the formulations (n = 3)

Formulation	Size (nm)	PDI	Zeta potential (mV)
Rk1-Lip	90.93 ± 1.52	0.218 ± 0.029	−24.99 ± 1.43
Rk1/CTX-Lip	95.15 ± 2.11	0.250 ± 0.053	−24.78 ± 1.99
Chol/CTX-Lip	118.25 ± 3.06	0.231 ± 0.040	−18.84 ± 1.11
Rk1-Lip/C6	102.13 ± 2.75	0.286 ± 0.035	−20.81 ± 0.48
Chol-Lip/C6	113.81 ± 1.89	0.198 ± 0.078	−22.46 ± 0.67
Rk1-Lip/IR-783	113.56 ± 2.93	0.301 ± 0.040	−24.24 ± 0.37
Chol-Lip/IR-783	124.79 ± 2.46	0.267 ± 0.036	−27.35 ± 0.75

CTX: Cabazitaxel; PDI: Poly dispersity index; Rk1/CTX-Lip: CTX-loaded liposomes modified with ginsenoside Rk1.

Rk1/CTX-Lip had satisfactory encapsulation efficiency (97.24 ± 0.75)% and a controlled release rate *in vitro*, as measured by HPLC (Figure 1C). Liposome stability was determined, and the particle size and encapsulation rates of the liposomes did not change significantly within 72 h (Figure 1D–E). In summary, these results indicated that ginsenoside Rk1 greatly improved the encapsulation efficiency and physical stability of liposomes.

Rk1/CTX-Lip can escape macrophage phagocytosis and effectively target tumor tissue

The biological functions of liposomes, including long circulation time and tumor-targeting abilities *in vivo*, were investigated. Qualitative observations using fluorescence microscopy and quantitative flow cytometry demonstrated that Rk1-Lip/C6 could escape macrophage phagocytosis and promote targeted uptake by RM-1 cells *in vitro* (Figure 2A–B). In the pharmacokinetic study, the blood CTX circulation time in the Rk1/CTX-Lip group was more efficient than that in the CTX-Sol group (Figure 2C). *In vivo* and *ex vivo* imaging further demonstrated the tumor-targeting ability of Rk1-Lip. Quantification of the imaging data revealed that the radiance intensity of Rk1-Lip/IR-783 was over two times greater than that of Chol-Lip/IR-783 in the tumor tissues at the observed time points (Figure 2D–G). These results were substantiated by fluorescence imaging of the tumor tissue slices (Figure 2H) and tissue distribution analysis (Figure 2I). The enhanced tumor-targeting ability may be attributed to the exposed Rk1 glycosides of the liposomes, which reduce the adhesion of plasma proteins, prolonging the circulation time of Rk1-Lip. Additionally, Rk1-Lip bind to the GLUT1 protein, highly expressed in tumor cells, promoting Rk1-Lip accumulation in tumor tissues[25].

Rk1/CTX-Lip exhibited potent antitumor efficacy and relieved concurrent infection burden

Ginsenoside Rk1 can inhibit tumor growth by promoting tumor cell apoptosis, increasing autophagy, and inhibiting tumor angiogenesis. Additionally, Ginsenoside Rk1 can improve immunity by enhancing cellular and humoral immunity[26,27]. The RM-1 cell viability of drug-loaded liposomes and free drugs was evaluated using the MTT assay, and the results showed that CTX + Rk1 exerted a stronger cytotoxic effect on RM-1 cells, suggesting a synergistic effect in the inhibition of RM-1 cell viability (Figure 3A and Table 2). To assess

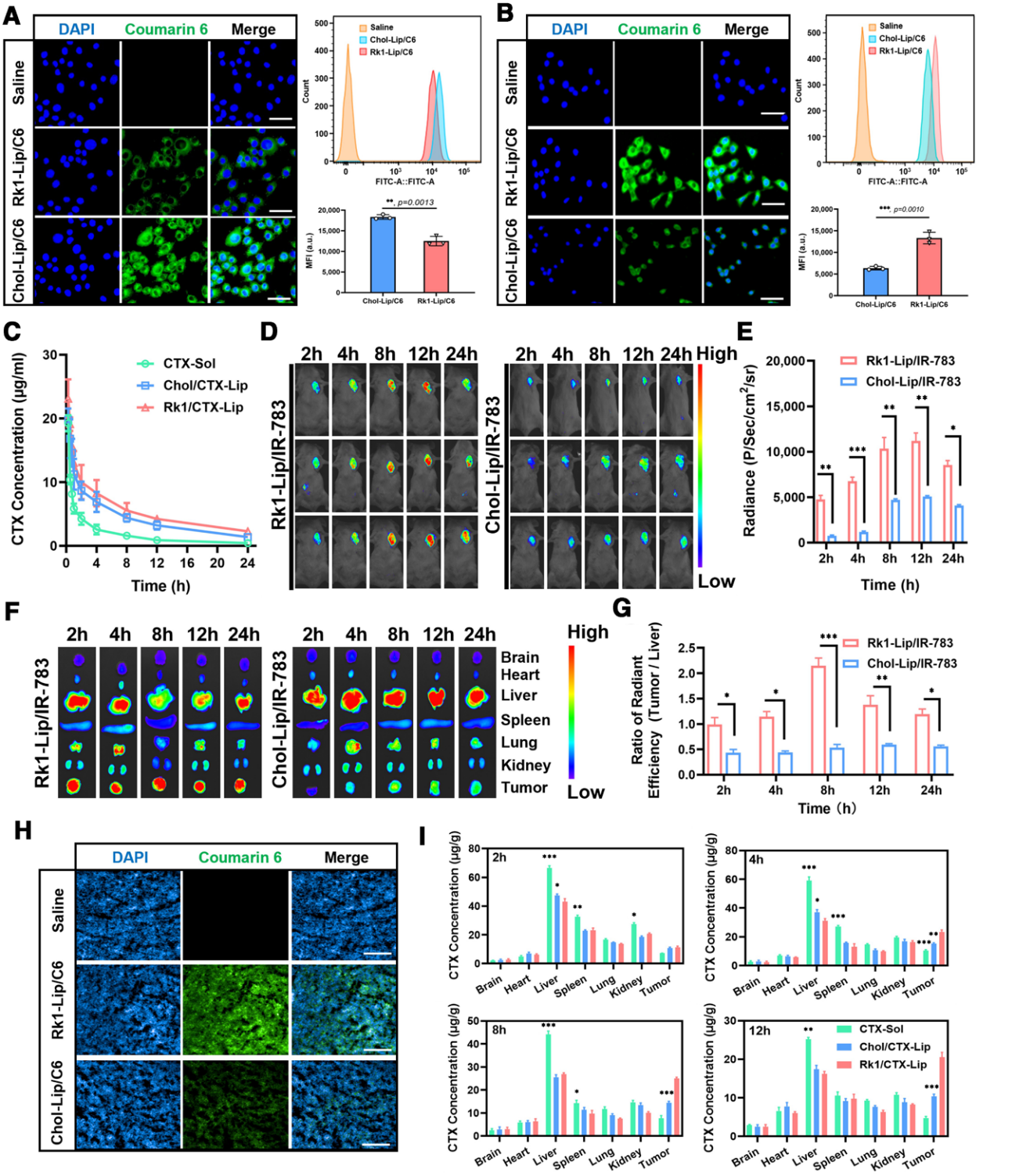

Figure 2. Evaluation of the biological functions of Rk1/CTX-Lip. (A–B) Uptake of saline, Rk1-Lip/C6, and Chol-Lip/C6 by (A) RAW264.7 macrophages and (B) RM-1 cells, scale bar = 50 μm. The fluorescence intensity measured by flow cytometry. (C) Plasma CTX concentration in SD rats after i.v. administration of CTX-Sol, Chol/CTX-Lip, and Rk1/CTX-Lip, respectively. (D) *In vivo* targeting ability of Rk1-Lip/IR-783 in tumor-bearing mice models and fluorescence intensity (E) determined by live imaging. (F) *Ex vivo* targeting ability of Rk1-Lip/IR-783 in tumor-bearing mice models determined by live imaging. (G) The semi-quantitative analysis of the ratio of fluorescence intensity (tumor/liver) of *ex vivo* imaging. (H) Representative fluorescent images in tumor slices after treatment of saline, Rk1-Lip/C6, and Chol-Lip/C6, scale bar = 50 μm. (I) *In vivo* biodistribution of formulations in tumor-bearing mice models at different time point after i.v. injection of CTX-Sol, Chol/CTX-Lip, and Rk1/CTX-Lip. Data are presented as mean ± SD ($n = 3$) (*$P < 0.05$, **$P < 0.01$, ***$P < 0.001$, compared with Rk1/CTX-Lip). CTX: Cabazitaxel; NS: Non-significance; Rk1/CTX-Lip: CTX-loaded liposomes modified with ginsenoside Rk1; SD: Standard deviation.

the maximum antitumor potential *in vivo*, the RM-1 subcutaneous xenograft mouse model was left untreated until the tumor volume reached ~100 mm^3. Then, the mice were dosed (15 mg/kg CTX) on days 1, 5, 9, and 13, and sacrificed on days 20 [Supplementary Figure S2, http://links.lww.com/AHM/A91]. Rk1/CTX-Lip exhibited substantial suppression of tumor growth, achieving over a 50% reduction in the average tumor volume

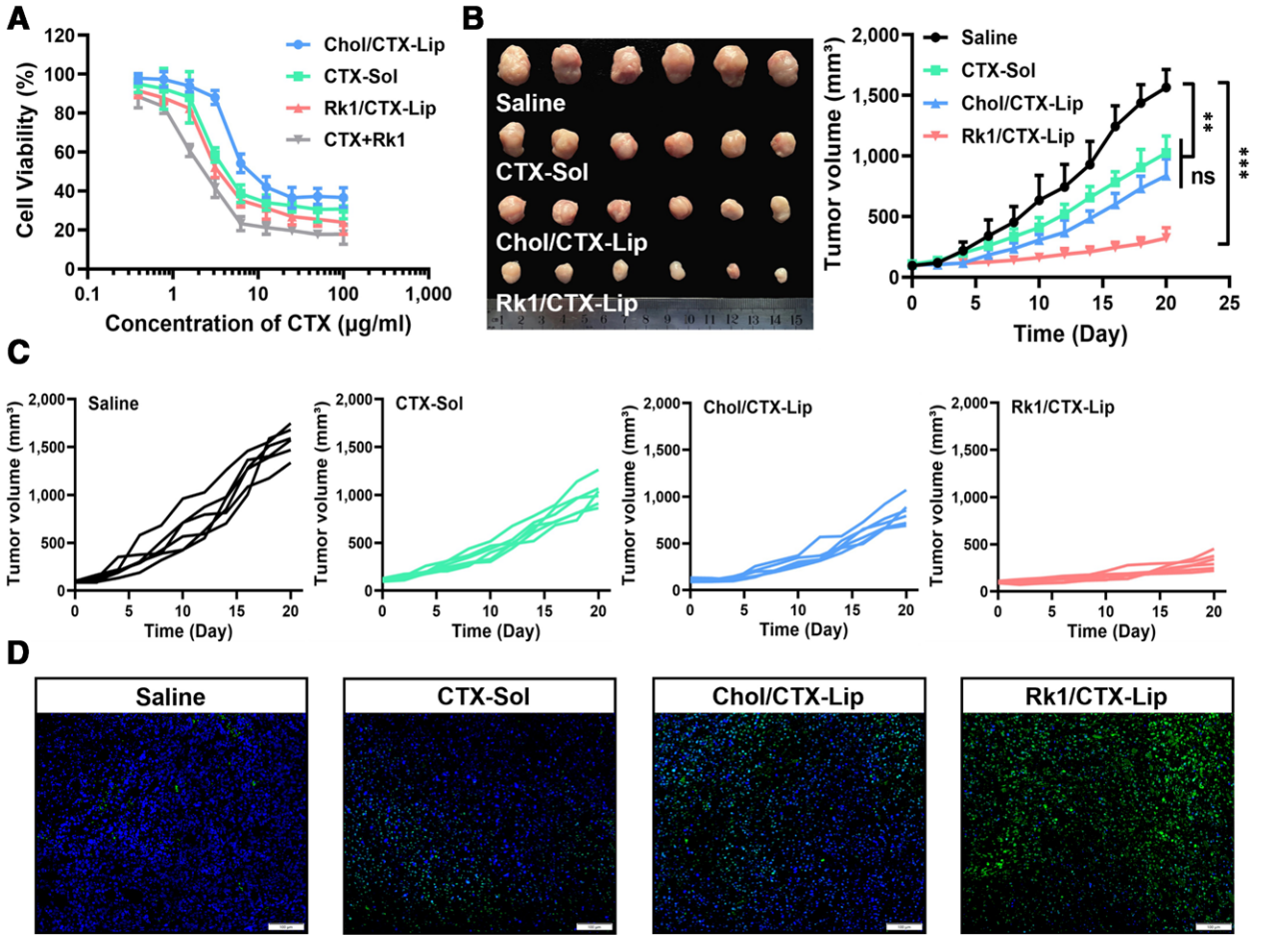

Figure 3. Investigation of the antitumor efficacy of Rk1/CTX-Lip. (A) *In vitro* antitumor activity test of Rk1/CTX-Lip. (B) The picture of tumor tissues and average tumor growth curves after the treatment. (C) Individual tumor growth curves in each group. (D) Analysis of apoptosis by TUNEL staining in tumor tissues in different groups, normal cell nuclei are stained blue and apoptotic cell nuclei are stained green. Data represented as mean ± SD ($n = 6$) (**$P < 0.01$, ***$P < 0.001$). CTX: Cabazitaxel; NS: Non-significance; Rk1/CTX-Lip: CTX-loaded liposomes modified with ginsenoside Rk1; SD: Standard deviation.

Table 2

***In vitro* antitumor activity test of Rk1/CTX-Lip and other formulations ($n = 6$)**

Formulation	IC_{50} (μg/mL)
CTX + Rk1	1.931 ± 0.14
CTX-Sol	2.891 ± 0.36
Rk1/CTX-Lip	2.789 ± 0.27
Chol/CTX-Lip	4.907 ± 0.31

CTX: Cabazitaxel; IC_{50}: Half-maximal inhibitory concentration; Rk1/CTX-Lip: CTX-loaded liposomes modified with ginsenoside Rk1.

compared with the Chol/CTX-Lip group (Figure 3B–C). TUNEL staining revealed that tumor cells in the Rk1/CTX-Lip group underwent apoptosis (Figure 3D). The apoptotic effect was attributed to the fact that Rk1-modified liposomes could effectively deliver CTX to tumor tissues and exert a synergistic antitumor effect.

The risk of life-threatening invasive fungal infections has been increasing for decades, with *Candida albicans* infections being the most prevalent, partly attributed to the use of chemotherapy drugs[10–12]. Therefore, the influence of Rk1/CTX-Lip on the risk of pathogen infection was explored in RM-1 tumor-bearing model mice, and *C. albicans* was used as the model pathogen. The presence of *C. albicans* was observed in the saline, CTX-Sol, and Chol/CTX-Lip groups upon infection. Notably, the Rk1/CTX-Lip group showed one and two orders of magnitude fewer CFUs on days 3 and 7 after infection, respectively [Supplementary Figure S3A–B, http://links.lww.com/AHM/A91]. These results demonstrate that Rk1/CTX-Lip exerted potent antitumor efficacy and relieved the concurrent infection burden.

Rk1/CTX-Lip can effectively regulate immune organs and cells and has superior biocompatibility

The spleen and thymus play crucial roles as immune organs in the human body for lymphocyte differentiation, maturation, and the immune response. Spleen and thymus indices can reflect and predict the immune function of the body[28]. In our study, no significant difference was observed in the spleen and thymus indices in the Rk1/CTX-Lip group compared to the saline group, whereas these indices were significantly decreased in the CTX-Sol and Chol/CTX-Lip groups (Figure 4A–B).

Lymphocytes play important roles in maintaining immune homeostasis and regulating systemic inflammatory responses[29,30]. Compared to the saline group, CTX-Sol markedly reduced the proportion of $CD4^+$ and $CD8^+$ T cells in the spleens of mice, whereas no

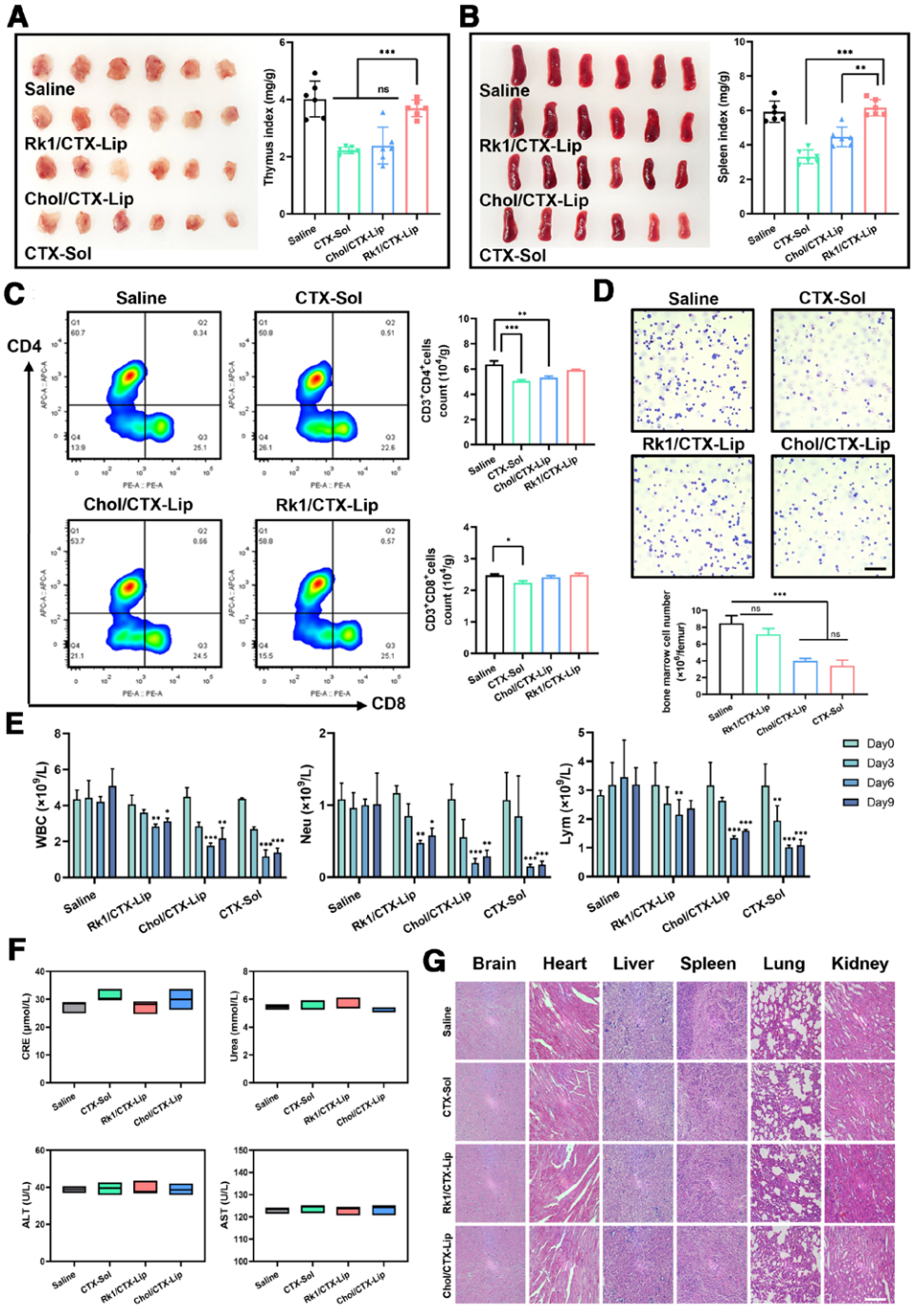

Figure 4. Modulatory effects in immune organs and cells and *in vivo* safety assessment of Rk1/CTX-Lip. (A–B) Thymus (A) and spleen (B) index of RM-1 xenograft model mice after treatments. (C) Flow cytometry plots and quantification of $CD3^+CD8^+$ and $CD3^+CD4^+$ T cells in spleen tissues. (D) Myelosuppression in mice. Bone marrow cells smear and bone marrow-nucleated cells count. (E) Hematology assessments of WBC, Neu, and Lym. (F) CRE, Urea, ALT, and AST indexes of RM-1 xenograft model mice after treatments. (G) H&E staining of the main organs in mice with different treatments (saline, CTX-Sol, Rk1/CTX-Lip, and Chol/CTX-Lip), scale bar = 200 μm. Data represented as mean ± SD ($n = 6$) (*$P < 0.05$, **$P < 0.01$, ***$P < 0.001$). ALT: Alanine aminotransferase; AST: Aspartate aminotransferase; CRE: Creatinine; CTX: Cabazitaxel; H&E: Hematoxylin and eosin; Lym: Lymphocytes; Neu: Neutrophils; NS: Non-significance; Rk1/CTX-Lip: CTX-loaded liposomes modified with ginsenoside Rk1; SD: Standard deviation; Urea: Urea nitrogen; WBC: White blood cells.

significant difference was observed in the Rk1/CTX-Lip group (Figure 4C). In contrast to the CTX-Sol and Chol/CTX-Lip groups, the number of bone marrow-nucleated cells in the Rk1/CTX-Lip group did not differ from that in the saline group (Figure 4D and Table 3). As a highlighted concern in the clinical application of CTX therapies, hematotoxicity has become the focus of safety inspection[31,32]. Rk1/CTX-Lip exhibited robust *in vivo* protection against hematological toxicity. The changes in white blood cells (WBCs), neutrophils (Neus), and lymphocytes (Lyms) were monitored on days 0, 3, 6, and 9 after treatment initiation, and severe hematotoxicity was observed in the CTX-Sol group with an approximately 50% to 70% reductions in abovementioned indicators (Figure 4E). Eliciting no significant physiological or histopathological

Table 3

Nucleated cell counts in the bone marrow of mice in different treatments (n = 6)

Group	Nucleated cell counts (×10^6/femur)
Saline	8.48 ± 0.89
CTX-Sol	3.41 ± 0.68
Chol/CTX-Lip	3.98 ± 0.31
Rk1/CTX-Lip	7.16 ± 0.70

CTX: Cabazitaxel; Rk1/CTX-Lip: CTX-loaded liposomes modified with ginsenoside Rk1.

changes in mice assessed through serum biochemical parameters (Figure 4F) or H&E staining of major organs (Figure 4G), Rk1/CTX-Lip exhibited superior biocompatibility.

Discussion

More than 80% of patients with cancer undergoing CTX treatment experience multiple symptoms, such as nausea, vomiting, leukopenia, and neutropenia[6–8]. Liposomes reduce drug toxicity and degradation owing to the presence of a lipid bilayer and reduce drug inactivation owing to their enhanced carrying capacity[33,34]. CTX-loaded liposomes were prepared by replacing cholesterol with the ginsenoside Rk1, which has a steroid structure similar to that of cholesterol with attached sugar moieties[20]. The modification prevented liposomes from interacting with various components of serum, reduced the adhesion of plasma proteins, and enabled favorable tumor-targeting ability and long circulation time *in vivo*. Rk1 and CTX exhibited synergistic antitumor effects and significantly reduced systemic toxicity during treatment. Combining natural products with current chemotherapeutic drugs possess the potential to improve therapeutic effects and reduce toxicity of chemotherapeutic drugs.

Similar to other chemotherapeutic drugs, the use of CTX in tumor treatment is not exempt from concerns about increased pathogen infection risks, contributing to significant morbidities and mortalities[35–38]. Accordingly, a *C. albicans* infection model was introduced in this study, and the substantial reduction in the occurrence of infections by Rk1/CTX-Lip was confirmed. The treatment of malignant tumors demands a comprehensive approach. Given the heightened risk of serious infections in patients with cancer, a more comprehensive treatment evaluation should be performed. Such evaluation should account for the occurrence of infections during antitumor therapy and aim to predict the subsequent medical prognosis accurately. Therefore, a limitation of the present study is to achieve an approximation of the preclinical cancer models which can more closely mimic the clinical reality.

Conclusion

In summary, we developed a CTX-loaded liposome modified with ginsenoside Rk1 (Rk1/CTX-Lip) with high CTX encapsulation efficiency and physical stability. Analysis of cell-derived xenograft models showed that Rk1/CTX-Lip could evade phagocytosis by macrophages, effectively target tumor tissues, exert strong antitumor effects, and reduce the burden of concurrent infections. Additionally, Rk1/CTX-Lip could effectively regulate immune organs and cells, and demonstrated superior biocompatibility. The use of Rk1/CTX-Lip is expected to offer novel approaches for the treatment of prostate cancer. Additionally, it presents innovative strategies to foster clinical advancement. Consequently, we anticipate that our investigation will contribute significantly to the fields of biology, materials science, chemistry, and medicine.

Conflict of interest statement

The authors declare no conflict of interest.

Funding

This work was supported by the National Natural Science Foundation of China (82373808), Chongqing Natural Science Foundation (cstc2021jcyj-bshX0125). Fundamental Research Funds for the Central Universities (SWURC2020001), the project for Chongqing University Innovation Research Group, Chongqing Education Committee (CXQT20006).

Author contributions

Chong Li, Feiyan Gao, and Dandan Huang conceived the project, designed all the experiments, analyzed the data, and wrote the manuscript. Zhongjie Tang and Xiao Pu conducted the experiments and analyzed the data. All authors edited the manuscript.

Ethical approval of studies and informed consent

The laboratory animal facility has been accredited by the IACUC (Institutional Animal Care and Use Committee) of Southwest University Laboratory Animal Center (IACUC Issue No. IACUC-20200905-02). All animal experiments were conducted under the guidelines of the Ethical Review Committee of experimental animals at the Southwest University of China.

Acknowledgments

The authors would like to thank the Academy of Agricultural Sciences, Southwest University for providing access to instrumentation and technical support.

Data availability

All data generated or analyzed during this study are included in this published article and its supplementary information files.

References

[1] Hoang B, Ernsting MJ, Tang WHS, et al. Cabazitaxel-conjugated nanoparticles for docetaxel-resistant and bone metastatic prostate cancer. *Cancer Lett* 2017;410:169–179.
[2] Hongo H, Kosaka T, Oya M. Analysis of cabazitaxel-resistant mechanism in human castration-resistant prostate cancer. *Cancer Sci* 2018;109(9):2937–2945.
[3] Song YZ, Tian QJ, Huang ZJ, et al. Self-assembled micelles of novel amphiphilic copolymer cholesterol-coupled F68 containing cabazitaxel as a drug delivery system. *Int J Nanomedicine* 2014;9:2307–2317.

[4] Martin SK, Pu H, Penticuff JC, et al. Multinucleation and mesenchymal-to-epithelial transition alleviate resistance to combined cabazitaxel and antiandrogen therapy in advanced prostate cancer. *Cancer Res* 2016;76(4):912–926.

[5] Yin XY, Luo LH, Li W, et al. A cabazitaxel liposome for increased solubility, enhanced antitumor effect and reduced systemic toxicity. *Asian J Pharm Sci* 2019;14(6):658–667.

[6] de Bono JS, Oudard S, Ozguroglu M, et al. Prednisone plus cabazitaxel or mitoxantrone for metastatic castration-resistant prostate cancer progressing after docetaxel treatment: a randomised open-label trial. *Lancet* 2010;376(9747):1147–1154.

[7] Lombard AP, Liu CF, Armstrong CM, et al. ABCB1 mediates cabazitaxel-docetaxel cross-resistance in advanced prostate cancer. *Mol Cancer Ther* 2017;16(10):2257–2266.

[8] Paller CJ, Antonarakis ES. Cabazitaxel: a novel second-line treatment for metastatic castration-resistant prostate cancer. *Drug Des Devel Ther* 2011;5:117–124.

[9] Gazendam RP, van de Geer A, van Hamme JL, et al. Impaired killing of Candida albicans by granulocytes mobilized for transfusion purposes: a role for granule components. *Haematologica* 2016;101(5):587–596.

[10] Lehrnbecher T, Frank C, Engels K, et al. Trends in the postmortem epidemiology of invasive fungal infections at a university hospital. *J Infect* 2010;61(3):259–265.

[11] McNeil MM, Nash SL, Hajjeh RA, et al. Trends in mortality due to invasive mycotic diseases in the United States, 1980-1997. *Clin Infect Dis* 2001;33(5):641–647.

[12] Enoch DA, Ludlam HA, Brown NM. Invasive fungal infections: a review of epidemiology and management options. *J Med Microbiol* 2006;55(Pt 7):809–818.

[13] Alaarg A, Jordan NY, Verhoef JJF, et al. Docosahexaenoic acid liposomes for targeting chronic inflammatory diseases and cancer: an *in vitro* assessment. *Int J Nanomedicine* 2016;11:5027–5040.

[14] Behzadi S, Serpooshan V, Tao W, et al. Cellular uptake of nanoparticles: journey inside the cell. *Chem Soc Rev* 2017;46(14):4218–4244.

[15] Kim YJ, Kwon HC, Ko H, et al. Anti-tumor activity of the ginsenoside Rk1 in human hepatocellular carcinoma cells through inhibition of telomerase activity and induction of apoptosis. *Biol Pharm Bull* 2008;31(5):826–830.

[16] Ryoo N, Rahman MA, Hwang H, et al. Ginsenoside Rk1 is a novel inhibitor of NMDA receptors in cultured rat hippocampal neurons. *J Ginseng Res* 2020;44(3):490–495.

[17] Hu JN, Xu XY, Li W, et al. Ginsenoside Rk1 ameliorates paracetamol-induced hepatotoxicity in mice through inhibition of inflammation, oxidative stress, nitrative stress and apoptosis. *J Ginseng Res* 2019;43(1):10–19.

[18] Kang S, Min H. Ginseng, the 'Immunity Boost': the effects of Panax ginseng on immune system. *J Ginseng Res* 2012;36(4):354–368.

[19] Zheng SW, Zheng HS, Zhang R, et al. Immunomodulatory effect of ginsenoside Rb2 against cyclophosphamide-induced immunosuppression in mice. *Front Pharmacol* 2022;13:927087.

[20] Chen CF, Chiou WF, Zhang JT. Comparison of the pharmacological effects of Panax ginseng and Panax quinquefolium. *Acta Pharmacol Sin* 2008;29(9):1103–1108.

[21] Gallay J, de Kruijff B, Demel RA. Sterol-phospholipid interactions in model membranes. Effect of polar group substitutions in the cholesterol side-chain at C20 and C22. *Biochim Biophys Acta* 1984;769(1):96–104.

[22] Commander R, Wei C, Sharma A, et al. Subpopulation targeting of pyruvate dehydrogenase and GLUT1 decouples metabolic heterogeneity during collective cancer cell invasion. *Nat Commun* 2020;11(1):1533.

[23] Choi JS, Chun KS, Kundu J, et al. Biochemical basis of cancer chemoprevention and/or chemotherapy with ginsenosides (Review). *Int J Mol Med* 2013;32(6):1227–1238.

[24] Yallapu MM, Othman SF, Curtis ET, et al. Multi-functional magnetic nanoparticles for magnetic resonance imaging and cancer therapy. *Biomaterials* 2011;32(7):1890–1905.

[25] Hong C, Wang D, Liang JM, et al. Novel ginsenoside-based multifunctional liposomal delivery system for combination therapy of gastric cancer. *Theranostics* 2019;9(15):4437–4449.

[26] Patra S, Pradhan B, Nayak R, et al. Chemotherapeutic efficacy of curcumin and resveratrol against cancer: chemoprevention, chemoprotection, drug synergism and clinical pharmacokinetics. *Semin Cancer Biol* 2021;73:310–320.

[27] Lee Y, Park A, Park YJ, et al. Ginsenoside 20(R)-Rg3 enhances natural killer cell activity by increasing activating receptor expression through the MAPK/ERK signaling pathway. *Int Immunopharmacol* 2022;107:108618.

[28] Oh MJ, Choi HD, Ha SK, et al. Immunomodulatory effects of polysaccharide fraction isolated from Fagopyrum esculentum on innate immune system. *Biochem Biophys Res Commun* 2018;496(4):1210–1216.

[29] Liao D, Luo YP, Markowitz D, et al. Cancer associated fibroblasts promote tumor growth and metastasis by modulating the tumor immune microenvironment in a 4T1 murine breast cancer model. *PLoS One* 2009;4(11):e7965.

[30] Sam QH, Yew WS, Seneviratne CJ, et al. Immunomodulation as therapy for fungal infection: are we closer? *Front Microbiol* 2018;9:1612.

[31] Chen Y, Pan Y, Hu D, et al. Recent progress in nanoformulations of cabazitaxel. *Biomed Mater* 2021;16(3):032002

[32] Sun B, Lovell JF, Zhang Y. Current development of cabazitaxel drug delivery systems. *Wiley Interdiscip Rev Nanomed Nanobiotechnol* 2023;15(2):e1854.

[33] Mirzavi F, Barati M, Soleimani A, et al. A review on liposome-based therapeutic approaches against malignant melanoma. *Int J Pharm* 2021;599:120413.

[34] Kang JH, Jang WY, Ko YT. The effect of surface charges on the cellular uptake of liposomes investigated by live cell imaging. *Pharm Res* 2017;34(4):704–717.

[35] Diehl R, Ferrara F, Müller C, et al. Immunosuppression for in vivo research: state-of-the-art protocols and experimental approaches. *Cell Mol Immunol* 2017;14(2):146–179.

[36] Emadi A, Jones RJ, Brodsky RA. Cyclophosphamide and cancer: golden anniversary. *Nat Rev Clin Oncol* 2009;6(11):638–647.

[37] Yu GC, Zhao XL, Zhou J, et al. Supramolecular polymer-based nanomedicine: high therapeutic performance and negligible long-term immunotoxicity. *J Am Chem Soc* 2018;140(25):8005–8019.

[38] Angarone M. Fungal infections in cancer patients. *Cancer Treat Res* 2014;161:129–155.